



Intermittent fasting and caloric restriction interact with genetics to shape physiological health in mice

Guozhu Zhang,¹ Andrew Deighan,² Anil Raj,¹ Laura Robinson,² Hannah J. Donato,² Gaven Garland,² Mackenzie Leland,² Baby Martin-McNulty,¹ Ganesh A. Kolumam,¹ Johannes Riegler,¹ Adam Freund ,¹ Kevin M. Wright,^{1,*†} and Gary A. Churchill ^{2,*†}

¹Calico Life Sciences LLC, South San Francisco, CA 94080, USA and

²The Jackson Laboratory, Bar Harbor, ME 04609, USA

*Corresponding author: Calico Life Sciences LLC, 1170 Veterans Blvd., South San Francisco, CA 94080, USA. Email: wright@calicolabs.com (K.M.W.); The Jackson Laboratory, 600 Main St., Bar Harbor, ME 04609, USA. Email: gary.churchill@jax.org (G.A.C.)

[†]Co-senior authors.

Abstract

Dietary interventions can dramatically affect physiological health and organismal lifespan. The degree to which organismal health is improved depends upon genotype and the severity of dietary intervention, but neither the effects of these factors, nor their interaction, have been quantified in an outbred population. Moreover, it is not well understood what physiological changes occur shortly after dietary change and how these may affect the health of an adult population. In this article, we investigated the effect of 6-month exposure of either caloric restriction (CR) or intermittent fasting (IF) on a broad range of physiological traits in 960 1-year old Diversity Outbred mice. We found CR and IF affected distinct aspects of physiology and neither the magnitude nor the direction (beneficial or detrimental) of effects were concordant with the severity of the intervention. In addition to the effects of diet, genetic variation significantly affected 31 of 36 traits (heritabilities ranged from 0.04 to 0.65). We observed significant covariation between many traits that was due to both diet and genetics and quantified these effects with phenotypic and genetic correlations. We genetically mapped 16 diet-independent and 2 diet-dependent significant quantitative trait loci, both of which were associated with cardiac physiology. Collectively, these results demonstrate the degree to which diet and genetics interact to shape the physiological health of adult mice following 6 months of dietary intervention.

Keywords: intermittent fasting; caloric restriction; physiological health; gene × environment interaction; Diversity Outcross mice

Introduction

Dietary modifications are the most robust interventions known to increase organismal lifespan. Caloric restriction (CR) has been shown to increase lifespan in multiple species including yeast, worms, flies, rats, mice, and nonhuman primates (Heilbronn and Ravussin 2003; Kaeberlein *et al.* 2005; Colman *et al.* 2009; Mattison *et al.* 2017; Liang *et al.* 2018; Pifferi *et al.* 2019). Another dietary modification, intermittent fasting (IF), has been shown to increase lifespan in rodents (Goodrick *et al.* 1990). However, the beneficial effects of these dietary interventions are not universal and can be influenced by sex, genetic variation, and adaptation to the lab environment (Goodrick *et al.* 1990; Harper *et al.* 2006; Liao *et al.* 2010; Mitchell *et al.* 2016). Moreover, the timing and duration of dietary intervention can alter the magnitude of lifespan effects, with the greatest increase observed when CR is imposed early and maintained throughout life (Weindruch *et al.* 1982; Yu *et al.* 1985; Goodrick *et al.* 1990; Dhahbi *et al.* 2004). However, the age-specific genetic and physiological mechanisms that determine whether CR or IF will lengthen lifespan remain largely unknown.

Dietary intervention is hypothesized to extend lifespan by improving the physiological function of multiple systems, including but not limited to, metabolic, neurological, and cardiovascular (Bauer *et al.* 2004; Gredilla and Barja 2005; Patel *et al.* 2005; Halagappa *et al.* 2007; Colman *et al.* 2009; Ahmet *et al.* 2011; Gräff *et al.* 2013; Redman *et al.* 2018). In some instances, changes in gene expression, metabolite levels, and physiology occur shortly after the initiation of daily CR (Cao *et al.* 2001; Dhahbi *et al.* 2004; Mulligan *et al.* 2008; Bruss *et al.* 2010). Despite the large number of CR experiments, it is not well understood how diet and genetics shape early life changes in physiological traits and whether these changes may have lasting effects on lifespan.

In humans, the largest CR intervention trial published to date found that a 2-year 25% CR treatment in a population of middle-aged, nonobese individuals caused significant reductions to multiple cardiovascular and metabolic syndrome risk factors (Kraus *et al.* 2019). However, the effect of CR was not universally beneficial; participants in this trial experienced significant reductions in bone mineral density, muscle size and function (Villareal *et al.* 2006, 2016; Weiss *et al.* 2007). These studies demonstrate that CR

Received: April 23, 2021. Accepted: August 10, 2021

© The Author(s) 2021. Published by Oxford University Press on behalf of Genetics Society of America.

This is an Open Access article distributed under the terms of the Creative Commons Attribution-NonCommercial-NoDerivs licence (<https://creativecommons.org/licenses/by-nc-nd/4.0/>), which permits non-commercial reproduction and distribution of the work, in any medium, provided the original work is not altered or transformed in any way, and that the work is properly cited. For commercial re-use, please contact journals.permissions@oup.com

improved multiple aspects of physiological function while worsening others in a relatively healthy population. It remains to be determined whether this result is a generalizable feature of CR interventions and whether IF treatment would produce similarly heterogeneous physiological effects. In addition, it is unknown how genetic variation may contribute to the variation in the physiological response to dietary intervention.

We investigate the effect of both CR and IF on a range of physiological traits using Diversity Outbred (DO) mice (*Mus musculus*), a multi-parent genetic mapping population founded from eight inbred strains (Churchill et al. 2012; Svenson et al. 2012). Our goal is to identify how dietary interventions affect different aspects of physiology in adult mice. We measure the effect of CR and IF on 36 morphological and functional traits derived from six phenotypic assays: grip strength, rotarod, dual-energy X-ray absorptiometry (DEXA), echocardiogram, acoustic startle, and wheel running. Many traits change significantly in 1-year-old mice exposed to dietary intervention for 6 months. The correlated change in trait values enabled us to cluster traits into distinct axes of physiology and measure how they were altered in response to dietary intervention. A significant proportion of phenotypic variation in 30 traits is heritable and for many traits in the same cluster, a large proportion of the heritable variation the genetic effects are correlated. We map 16 diet-independent quantitative trait loci (QTL) and two diet-dependent QTLs. We impute all DO founder variants, fine-map QTL intervals to near single gene resolution and identify the founder allele(s) associated with trait variation. These findings enable us to conclude that dietary intervention has heterogeneous effects on physiological health in adult mice, phenotypic variation in many physiological health traits has a large genetic component, and in the case of cardiac physiology, variation is influenced by the interaction between genetics and dietary intervention.

Study design and measurements

The DO mouse population was derived from eight inbred founder strains and is maintained at The Jackson Laboratory as an outbred heterozygous population (Svenson et al. 2012). This study contains 960 female DO mice, sampled at generations: 22–24 and 26–28. There were two cohorts per generation for a total of 12 cohorts and 80 animals per cohort. Enrollment occurred in successive quarterly waves starting in March 2016 and continuing through November 2017.

A single female mouse per litter was enrolled into the study after wean age (3 weeks old), so that no mice in the study were siblings and maximum genetic diversity was achieved. Mice were housed in pressurized, individually ventilated cages at a density of eight animals per cage (cage assignments were random). Mice were subject to a 12h:12h light:dark cycle beginning at 0600h. All animal procedures were approved by the Animal Care and Use Committee at The Jackson Laboratory.

From enrollment until 6 months of age, all mice were on an Ad Libitum diet of standard rodent chow 5KOG from LabDiet. At 6 months of age, each cage of eight animals was randomly assigned to one of five dietary treatments, with each cohort equally split between the five groups ($N = 192/\text{group}$): Ad Libitum (AL), daily 20% CR (20%), daily 40% CR (40%), 1 day per week fast (1D), and 2 days per week fast (2D) (see Figure 1).

Mice on AL diet had unlimited food access; they were fed when the cage was changed once a week. In rare instances when the AL mice consumed all food before the end of the week, the food was topped off mid-week. Fasting was imposed weekly from

Wednesday noon to Thursday noon for mice on 1D treatment and Wednesday noon to Friday noon for mice on 2D treatment. Mice on 1D and 2D diets have unlimited food access (similar to AL mice) on their nonfasting days. The IF regimens were chosen to mimic long periods of food deprivation that are typically experienced by animals in the wild (Anton et al. 2018). The 1D and 2D fast treatments were chosen to induce a starvation response in mice (Bauer et al. 2004).

CR was imposed with daily feeding of a pre-determined amount of food. We estimated the average food consumption of female DO mice from a study conducted at The Jackson Laboratory. We found the average mouse consumed 3.43g/mouse/day and set the 20% CR diet to be 2.75g/mouse/day and the 40% CR diet to be 2.06g/mouse/day. For these treatments, food was weighed out each weekday and on Friday afternoon these mice were given a triple feeding to last till Monday afternoon. Food was distributed based on the number of animals in each cage, which at the start of the experiment, contained eight mice. As the number of mice in each cage decreased over time, the amount of food given to each cage was adjusted to reflect the number of mice in that cage. Direct observation of 20% and 40% CR mice at feeding indicated that mice in a cage have approximately equal access to the food. We observed no hoarding and all food was usually consumed within 1–2h. The change in body weight following dietary intervention is consistent with our interpretation that all mice in a housing unit are experiencing some degree of CR (Supplementary Figure S1A). Nonetheless, individual feeding behavior was not controlled and it was possible that some of the variability observed in the CR treatment groups (Supplementary Figure S1, B–F) was due to varying degrees of individual caloric intake.

Phenotypic assays

We carried out six phenotypic assays to assess motor and neuromuscular function, activity, body composition, hearing, and cardiovascular physiology, at approximately 1 year of age, 5–6 months following dietary intervention (Figure 1). All assays were conducted at The Jackson Laboratory following standard operating procedures, described in Supplementary File S1.

The rotarod assay was run with three consecutive trials per animal and we derived three traits to measure each animal's latency to fall (Figure 1). The grip strength assay was run with three consecutive trials for all-paws and three trials for forepaws. In order to maximize the robustness of this assay, we removed any trial with log-normal Euclidean distance in the upper 5% quantile of the distribution of all animals and then calculated the per mouse average of the remaining trials. We used DEXA to quantify eight body and bone composition traits (Figure 1). We measured voluntary wheel running in 30 min intervals for three nights and 2 days (mice were single housed for this assay). We used these data to derive average distance, time spent running and max speed in the following intervals: 12h day, 12h night, and 24h intervals (Figure 1). The echocardiogram assay measured 11 traits capturing both heart morphology and function (Figure 1). Note, cardiac output is not directly measured, it is calculated from the product of stroke volume and heart rate.

The acoustic startle assay followed the sound-startle response protocol in which animals were exposed to five sound levels ranging from 80 to 120 decibels (dB) at 10 dB steps. Each animal's average startle response was normalized to background noise. To robustly measure hearing and sensorimotor function, we fit the startle response measurements for each animal to a five

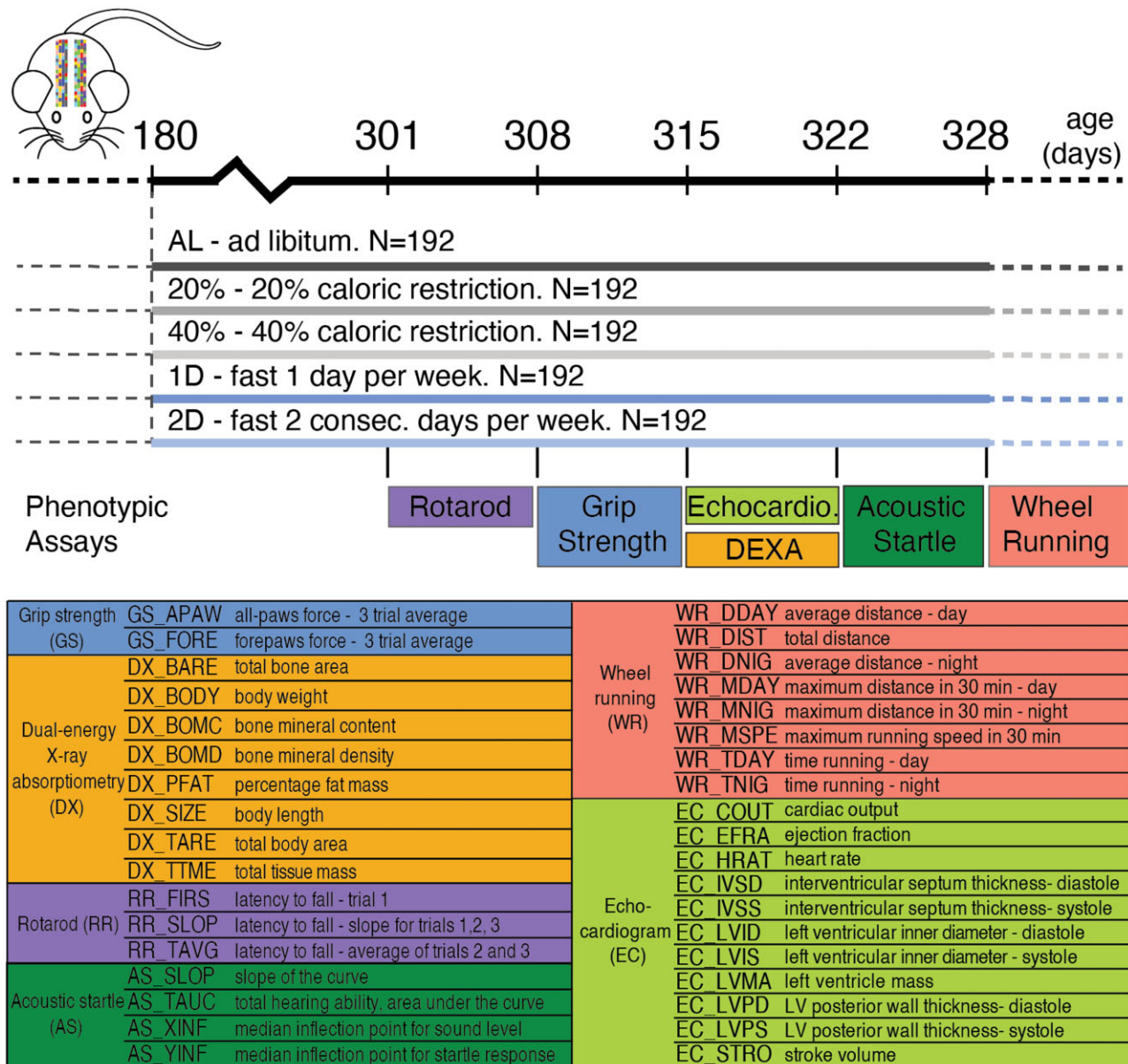


Figure 1 Study design. Dietary intervention starts at 180 days of age. Experimental procedures take approximately 1 week starting from given day.

parameter logistic model with the R package *nplr* (Commo and Bot 2016) and derived four values to quantify the shape of the logistic model (description provided in Figure 1). For a few animals, we estimated the median sound response value to be greater than 120 dB, the maximum sound level in our experiment. These values were set to 122 dB, which is twice as loud as 120 dB and is often used as the peak sound level in noise induced hearing loss research in rodent models (Kim et al. 2005; Escabi et al. 2019).

Quantify phenotypic effects following outlier detection and batch correction

We first identified technical outliers resulting from equipment failure or mislabeled animals and if we could not manually correct them using lab records, they were removed. The total number of samples per trait after outlier removal is listed in Supplementary Table S1. In order to prevent potential biases in interpretation and increase the reliability of these trait

measurements, we corrected values for batch and technician effects (Mandillo et al. 2008; Kafkafi et al. 2018; Gulinello et al. 2019). For this experiment, there were 12 batches (two for each DO generation) and eight technicians. To quantify batch and technician effects, we fit an analysis of variance (ANOVA) model as follows:

$$\text{Trait} = \text{Diet} + \text{Batch} + \text{Experimenter} + \text{Error}. \quad (1)$$

In contrast to all other assays, greater than 80% of echocardiogram derived traits were collected by a single technician and we determined that a reduced ANOVA model including Batch and not Experimenter terms was sufficient to control for the batch and technician effects. We used the residuals from each model to identify and remove biologically impossible values according to Tukey's rule for far outlier (Tukey 1977). After removing far outliers, we repeated the model fit procedure. To remove batch and

experimenter effects, we adjusted each trait using the batch and experimenter model coefficients.

Grip strength and rotarod derived traits can be confounded by body weight (Maurissen *et al.* 2003; Crawley 2007) and in order to account for this, we fit the following Analysis of Covariance (ANCOVA) model:

$$\text{Trait} = \text{Diet} + \text{Batch} + \text{Experimenter} + \text{Weight} + \text{Error}. \quad (2)$$

To remove body weight effect for grip strength and rotarod derived traits, we adjusted the trait value using the following formula:

$$\text{AdjTrait} = \text{Trait} - \text{Beta} * (\text{Weight} - \text{AveWeight}), \quad (3)$$

where Beta is the body weight coefficient from the ANCOVA model and AveWeight is the population mean body weight. Following technical, batch, technician, and outlier correction, we applied z-score standardization for all traits. Unless otherwise stated, these values were used for each subsequent analysis.

To quantify the effect of dietary intervention on each trait, we applied an ANOVA model with Dunnett *post-hoc* test to compare each diet intervention group to the AL group. In order to account for multiple statistical tests, we applied the Westfall-Young P-value adjustment and set the significance threshold to be 0.05 (Westfall *et al.* 1993).

Phenotypic correlation and unsupervised clustering analysis

We calculated correlation coefficients within each diet treatment, and experiment-wide correlation coefficients for all animals across all diets. We performed unsupervised hierarchical clustering analysis using the distance metric $1 - |\text{Phenotypic Correlation}|$ and complete linkage. For animals to be included in this hierarchical clustering procedure we required they had no missing trait data ($N = 525$). To determine cluster membership of each trait, we applied a sensitivity analysis by first calculating the within cluster similarity, *dist-within*, of a trait as the average pairwise distance to all other traits in the same cluster. Second, we calculated the across cluster similarity, *dist-across*, as the average pairwise distance to all traits outside of the cluster. Small values of *dist-within* indicate the trait is highly correlated with traits within the cluster, whereas large values of *dist-across* indicate the trait is highly uncorrelated with traits outside of the cluster. To identify robust clusters of highly correlated traits, the hierarchical clustering algorithm minimizes the penalty score, defined as *dist-within*/*dist-across*. This penalty score is sensitive to the size of the cluster and to derive a cluster size specific penalty significance threshold, we used a bootstrap method with 1000 resampling trials. The cluster size specific penalty significance threshold was defined as the 0.05/(cluster size-1) quantile value (Supplementary Table S2).

In order to organize traits into robust clusters, we first created a dendrogram with 5 clusters and compared the observed penalty scores to the bootstrap derived penalty threshold values. Within each cluster, we removed traits that had a higher penalty score than the penalty significance threshold by moving the cut-tree function closer to the origin node of the dendrogram. After the creation of a new set of clusters, we repeated the process until every newly created cluster had a penalty score that was less than the bootstrap derived penalty threshold values. We kept singletons, as single-trait clusters. Finally, we used principle component (PC) analysis of traits within the same multi-trait cluster to

derive composite traits. All PC derived traits with a cumulative of 90% total variance explained were included in genetic linkage analyses.

Genotype data and quality assessment

We collected tail clippings and extracted DNA using DNeasy Blood and Tissue Kit (Qiagen) from 954 animals. Note, six of the 960 animals that started the experiment died prior to collecting tail clippings. Samples were genotyped using the 143,259-probe GigaMUGA array from the Illumina Infinium II platform (Morgan *et al.* 2015) by NeoGen Corp. (genomics.neogen.com/, last accessed October 26, 2021). We evaluated genotype quality using the R package: *qtl2* (Broman *et al.* 2019). We processed all raw genotype data with a corrected physical map of the GigaMUGA array probes (https://kbroman.org/MUGAarrays/muga_annotations.html, last accessed October 26, 2021). After filtering genetic markers for uniquely mapped probes, genotype quality and a 20% genotype missingness threshold, our dataset contained 110,807 markers.

We next examined the genotype quality of individual animals. We found seven pairs of animals with identical genotypes which suggested that one of each pair was mislabeled. We identified and removed a single mislabeled animal per pair by referencing the genetic data against coat color. Next, we removed a single sample with missingness in excess of 20%. All remaining samples exhibited high consistency between tightly linked markers: log odds ratio error scores were less than 2.0 for all samples (Lincoln and Lander 1992). The final set of genetic data consisted of 946 mice.

For each DO mouse, we compared its genotype to that of the eight founder strains at all 110,807 markers to calculate the probability that a given founder contributed a given allele at that marker [implemented in the R package: *qtl2* Broman *et al.* (2019)]. In other words, the founder-of-origin probability is the likelihood a given DO mouse possesses a specific founder haplotype at the focal marker and can be used to identify genomic regions that are identical-by-descent. This allowed us to directly test for an association between the founder-of-origin probability and phenotype at all genotyped markers. Using the founder-of-origin of consecutive typed markers and the genotypes of untyped variants (SNPs and small insertion-deletions) in the founder strains, we then imputed the genotypes of all untyped variants (34.5 million) in all 946 mice. The majority, but not all, of imputed variants were bi-allelic SNPs. Targeted association testing at imputed variants allowed us to fine-map many QTLs to near single gene resolution.

Genetic linkage analysis

With the R *qtl2* package, we calculated kinship matrices using the leave-one-chromosome-out (LOCO) method and conducted quantitative trait locus mapping analyses (Broman *et al.* 2019). In order to identify significant additive genetic associations, we fit a linear mixed model with diet and founder-of-origin probabilities per marker as fixed effects and kinship as a random effect. To identify significant genotype by diet (GxD) interaction effects, we fit a linear mixed model with diet and founder-of-origin probabilities and their interactions as fixed effects and kinship as a random effect. To calculate an LOD score for the GxD interaction term we subtracted the LOD score of the full model from the additive model. To determine whether the interaction LOD score was statistically significant, we conducted a permutation analysis by randomizing phenotype values (regardless of dietary treatment), fitting both the full and the

additive models, subtracting the genome wide set of LOD scores of the full model from the additive model and storing the maximum LOD value (Churchill and Doerge 1994). We repeated this procedure 1000 times to obtain a distribution of maximum LOD scores and applied empirical P-value threshold of 0.05 to define significant QTLs and 0.1 as suggestive QTLs.

For each significant and suggestive QTL, we used the founder-of-origin probabilities to impute all variants identified in the fully sequenced founder lines for 5 Mb \pm the lead marker position Gatti et al. (2014); Oreper et al. (2017) and re-ran the QTL mapping procedure [implemented in the `snpscan` function from `qtl2`, Broman et al. (2019)]. To assess the significance of imputed variants for each region, we re-ran the permutation procedures as previously described with 1000 iterations and applied empirical P-value threshold of 0.05. To more precisely fine-map each QTL, we identified all candidate variants as those that are specific to lead founder-allele-pattern (FAP), or if the lead FAP contains fewer than 10 variants, we also include variants specific to the second-ranked FAP (Wright et al. 2020). We identified lead candidate genes by their proximity to candidate FAP variants and by cross-referencing against phenotypic effect in the Mouse Genome Informatics (www.informatics.jax.org) database.

Heritability and genetic correlations analyses

For each trait, we calculated the additive genetic variance relative to phenotypic variance, e.g., narrow-sense heritability, and its 95% credible interval using a Bayesian model with diet as a fixed effect and kinship as a random effect based on the EMMA model as implemented in R's STAN package (Kang et al. 2008; Carpenter et al. 2017; Stan Development Team 2020). We assessed whether heritability was significantly greater than zero by applying one-sided z-test to the posterior distribution with false discovery rate controlled at 0.05.

To measure the degree to which the additive genetic variance underlying two traits is shared we calculated their genetic correlation using the mathematical framework described in Furlotte and Eskin (2015). We used a Bayesian model implemented in R's STAN package (Stan Development Team 2020) to estimate the genetic correlation and its 95% credible interval. The details about model assumptions and priors are in the Supplementary Materials. We ran three independent chains with 2,000 Markov chain Monte Carlo (MCMC) iterations, and posterior estimates were derived by combining all three MCMC chains after 1000 burn-ins. The convergence diagnostics were assessed by Gelman-Rubin's statistic (Gelman and Rubin 1992). The significance of phenotypic correlation was determined by t-test and the significance of genetic correlation was determined by posterior mean and standard deviation under standard normal distribution. We applied Benjamini and Hochberg (1995) method to control significant phenotypic and genetic correlations respectively, at a false discovery rate of 0.05.

Comparison of full and reduced genotype-by-diet association models to measure interaction effects

In order to determine which diet intervention(s) are responsible for genotype-by-diet interaction effects, we re-tested the lead genotypic marker at each significant QTL in the following models:

$$\begin{aligned} \text{Null} : T &= D_{\text{Full}} + G + G * D_{\text{Full}} + K + e \\ \text{Alternative} : T &= D_{\text{Full}} + G + G * D_{\text{Reduced}} + K + e, \end{aligned}$$

where T is trait, G is genotype, K is kinship, e is error, D_{Full} is all

five treatments and D_{Reduced} eliminates, in singles or pairs, 1D fast, 2D fast, 20% CR, or 40% CR. We first remove a single diet at a time and evaluate the fit of each alternative model using the likelihood ratio test. The diet with the highest LOD score is then tested in pairs with each of the other three diets to determine whether model fit is improved.

Results

Dietary intervention altered physiology of adult mice

We measured the effect of dietary interventions on multiple aspects of mouse physiology and found that both the type (CR vs IF) and magnitude of each intervention affected the physiological response. To summarize, the 40% CR intervention had the greatest impact, 24 of 36 total traits were significantly different compared to the AL diet (Figure 2). For a subset of traits, we also provide the non z-score transformed values (Supplementary Figure S2). Following the 40% CR intervention, the 20% CR, 2D fast, and 1D fast treatments resulted in 11, 9, and 4, traits changing significantly in comparison to the AL group (Figure 2). Body weight was significantly reduced in all four treatments, with the largest effect observed in 40% CR treatment [DX_BODY, Figure 2; Supplementary Figure S1; Wright et al. (2020)]. In fact, the 40% CR treatment resulted in the largest changes for all body and bone composition traits (body length, percent fat mass, tissue mass, tissue area, bone area, bone mineral density, and bone mineral content) and the effects were often more than double those observed in the 20% CR treatment (Figure 2). Interestingly, the 2D fast and 20% CR had nearly the same mean body weights, however the treatments exhibited opposite effects on body fat percentage: 2D fast reduced and 20% CR increased DX_PFAT (Figure 2). In summary, IF and daily CR had distinct effects on multiple body and bone composition traits and changes in response to the 40% CR and 2D fast treatments were not simply a doubling of magnitude of 20% CR and 1D fast treatment effects. These patterns were also observed for additional physiological traits.

We identified multiple cardiac phenotypes which were significantly altered by both the 20% CR and 40% CR treatments. Heart rate, cardiac output, and diastolic left ventricle wall thickness (EC_HRAT, EC_COUT, and EC_LVPD) were significantly lower in both CR groups compared to AL (Figure 2). In addition, the 20% CR group exhibited significantly lower systolic left ventricle wall thickness (EC_LVPS) and stroke volume (EC_STRO) whereas the 40% CR group exhibited significantly lower left ventricle mass and inner dimension in systole and diastole (EC_LVMA, EC_LVIS, and EC_LVID). The cumulative effect of these divergent responses was that the 20% CR group had the lowest ejection fraction and the 40% CR group had the highest ejection fraction (Figure 2, EC_EFRA). Similarly, after controlling for body weight, we found stroke volume and cardiac output was lowest for the 20% CR group and highest for the 40% CR group (Supplementary Figure S2 E, F, I, and J). These results suggested that CR was detrimental to the cardiovascular efficiency of adult mice treated with 20% CR and beneficial to the 40% CR group. This pattern of effects was similar to the effect on percent fat mass, in which 20% CR, and 40% CR treatment effects relative to AL varied in both magnitude and sign (positive or negative).

The effects of IF were more subtle than CR on the cardiac traits and though these changes were not statistically significantly different between 1D fast or 2D fast and AL, we observed a number of interesting trends (Figure 2). We found the 2D fast

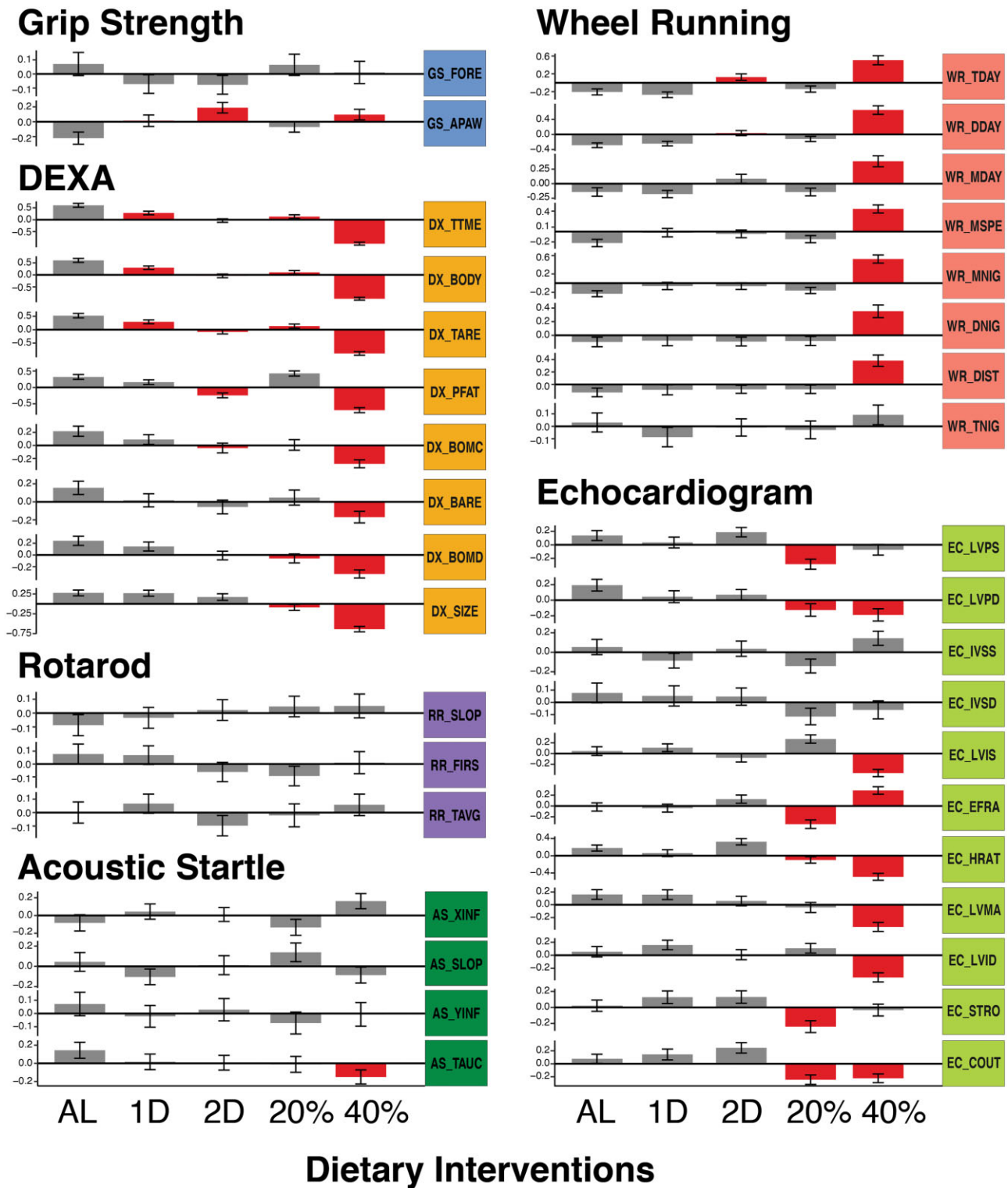


Figure 2 Diet specific mean (SE) trait values for all experimental procedures. All trait values were z-score transformed following batch and generation correction. Red bars denote traits that were significantly different from AL diet at a Westfall-Young multiple tests adjusted *P*-value threshold of 0.05.

treatment increased stroke volume and ejection fraction, similar to 40% CR and in contrast with 20% CR. The 2D fast treatment also resulted in increased systolic and diastolic left ventricle wall thickness, which contrasted with both the 20% CR and 40% CR treatments (Figure 2).

We conducted multiple experiments to measure neuromuscular and motor function: running on a wheel, grip strength, and

balancing on the rotarod. Wheel running activity, measured as total distance, max speed, and amount of time on a running wheel, were significantly increased in the 40% CR treatment compared to all other groups for both the light and dark cycles (Figure 2). The 2D fast treatment exhibited a significant increase in total wheel time and moderate increases in distance and max speed during the day compared to the other groups (Figure 2). No

wheel running traits were significantly different in the 1D fast or 20% CR treatments in comparison to the AL group (Figure 2). The only significant difference observed among the grip strength and rotarod traits was an increase in all-paws grip strength with the greatest effects in the 2D fast followed by 40% CR treatments (Figure 2). To summarize the effect of dietary intervention on neuromuscular and motor function, 40% CR and 2D fast, in comparison to the other treatments, ran the farthest and had the greatest strength. Interestingly, these same groups had the lowest body weight and lowest body fat percentage.

We measured hearing ability using the acoustic startle experiment. We found the AL treatment had the most sensitive hearing whereas the 40% CR treatment mice had the least sensitive hearing, when measured as the total area under the startle response curve (AS_TUAC, Figure 2). This result suggested that 6-month exposure to 40% CR treatment, in contrast to all other interventions, had a detrimental effect on hearing ability in 12-month old mice.

Collectively, these results demonstrated that IF and daily CR had distinct effects on multiple aspects of physiology and neither the magnitude nor the sign of effects were linear with respect to daily calorie intake or length of IF regime. In addition, none of these interventions were universally beneficial across all aspects of organismal physiology. Finally, we found the effect of dietary intervention was correlated between many traits. In some instances, this was because one trait was directly calculated from another trait measured in the same assay (see Methods: Phenotypic Assays). Alternative and mutually nonexclusive hypotheses may also explain these results: (1) the traits measured similar aspects of physiology (e.g., fat mass and body weight), (2) the traits were derived from the same phenotypic assay and environmental variables (e.g., time of day, time of year, experimenter) were constant, and (3) trait variation is controlled by a shared genetic basis. In order to investigate these hypotheses, we estimated the heritability of each trait and their pairwise phenotypic and genetic correlations.

The majority of physiological traits exhibit significant genetic heritability

To determine the contribution of genetics to phenotypic variation in each trait irrespective of diet, we calculated heritability across all animals in the study and found that most traits measured at 1 year of age (31 of 36) have significant heritability (Figure 3). Body composition traits from DEXA and one measure of hearing sensitivity had the highest heritabilities (>0.5). Wheel running speed and distance traits had moderate (0.3–0.5) heritabilities. Several cardiac traits, including heart rate, stroke volume, and cardiac output, as well as forepaw grip strength and time to fall on the rotarod had low (0.1–0.3) but statistically significant heritabilities. Traits with heritability not significantly different from zero included two echocardiogram derived traits, and one each for acoustic startle, rotarod, and grip strength (Figure 3).

Phenotypic and genetic correlations separate distinct aspects of physiology

We calculated the phenotypic correlation between all trait pairs using all samples and found that many trait pairs derived from the same assay were tightly correlated. (Figure 4A, lower-triangle). In order to assess whether these correlations were altered by diet, we fit the following regression model:

$$\text{trait}_2 = \text{trait}_1 + \text{diet} + \text{trait}_1 : \text{diet}$$

and evaluated the statistical significance of the interaction term. We tested all trait pairs and none had a significant interaction

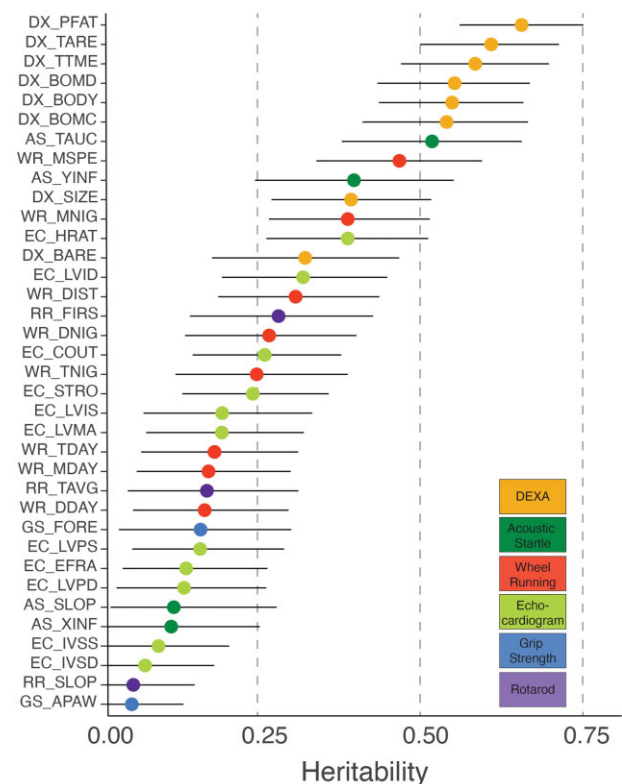


Figure 3 Trait specific heritability (95% Bayesian credible interval) values.

term at an FDR adjusted P -value less than 0.05 (Supplementary File S2). Moreover, we found diet-specific trait correlation values were generally unchanged between diets (Supplementary Figure S3). For example, cardiac output and stroke volume (EC_COUT, EC_STRO) were positively correlated with body composition traits (DX_PFBT, DX_TARE, DX_BODY, and DX_TTME) in AL, 1D and 2D group, however, the correlation was reduced in 20% CR and 40% CR groups (Supplementary Figure S3). Since the phenotypic correlations were largely similar across diets, we used correlations calculated from all animals in subsequent analyses.

In order to measure the degree to which the heritable fraction of variation in two traits was shared we calculated their genetic correlation (Figure 4A, upper-triangle). This value measures the correlation of genetic effects on two traits, and a genetic correlation equal to one means that every variant that affects the first trait has an equal pleiotropic effect on the second trait. For many traits, the genetic and phenotypic correlations were similar (adjusted R square of 0.62, Supplementary Figure S4). In addition, we identified 138 instances (out of 630 trait pairs) for which the phenotypic correlation was significantly greater than zero but the estimated genetic correlation was indistinguishable from zero. This suggested that, for these trait pairs, the phenotypic correlation was due to shared environmental factors.

We sought to quantify the degree of similarity between traits using an unsupervised hierarchical clustering analysis of all pairwise phenotypic correlations. To conduct this analysis, we used animals with complete data across all traits. The dietary treatment effects in this subset of animals (Supplementary Figure S5) were similar to the effects seen in the full cohort (Figure 2). We identified 10 clusters of two or more traits and six single-trait clusters (Figure 4B). All 10 multi-trait clusters were composed of traits from the same assay, however traits from all assays (except

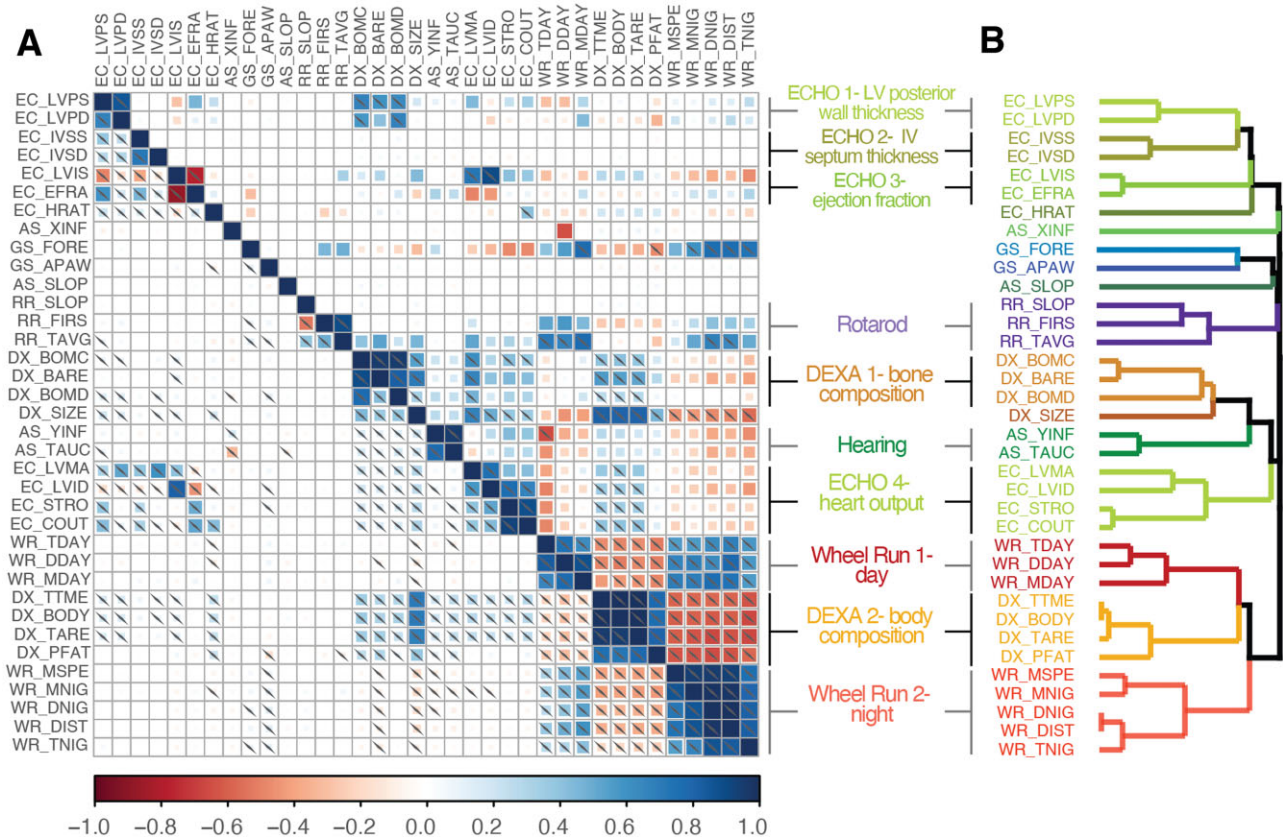


Figure 4 (A) Pairwise genetic (upper-triangle) and phenotypic (lower-triangle) correlations. Squares containing a back-slash highlight correlations with an FDR adjusted P -value < 0.05 . (B) Hierarchical clustering of traits based on phenotypic correlation values. Each color represents a significantly distinct cluster.

rotarod) were split across multiple clusters in nonadjacent regions of the dendrogram (Figure 4B). For example, DEXA derived body composition traits formed two multi-trait clusters. The first cluster was composed of bone physiology traits and was adjacent to a cardiac output cluster, whereas the second cluster was composed of body area/tissue composition traits and was located within day and night time wheel running clusters (Figure 4B). We interpret traits in distinct clusters as measurements of distinct aspects of physiology, with cluster placement in the dendrogram indicating the degree of similarity between these aspects of physiology.

Multiple factors may contribute to the high correlations within each multi-trait cluster: different traits measured the same underlying physiology, the shared environment in which traits were measured, and a shared genetic basis. In eight of 10 multi-trait clusters, nearly all trait pairs within each cluster were significantly genetically correlated with each other (Figure 4A), suggesting that the traits that comprise these aspects of physiology shared a common genetic basis. In the two remaining multi-trait clusters (Rotarod and ECHO 2), trait pairs were, for the most part, not significantly genetically correlated (Figure 4A) because of the low genetic heritability of one or both traits (Figure 3). This result suggested that the significant phenotypic correlations within these clusters was likely due to shared environmental factors.

Genetic mapping with founder-allele-patterns identifies candidate variants

We sought to measure the diet-independent and diet-dependent genetic basis of each directly measured trait using a QTL

mapping approach. Using both additive and genotype-by-diet (GxD) interaction models, we used the founder-of-origin genotype probabilities to map associations for each of the 36 directly measured traits. For the additive model, we found 16 significant QTLs (P -value < 0.05) and seven suggestive QTLs (P -value < 0.1) among the 36 phenotypic traits (Table 1). In instances in which multiple traits map to the same genomic region we count these as a single QTL. For the GxD interaction model, we identified two significant QTLs -both of which were associated with cardiac physiology traits- and one suggestive QTL for hearing sensitivity (Table 1).

To more thoroughly interrogate aspects of physiology represented by each multi-trait cluster, we conducted a principal component analysis of the traits in each cluster (Supplementary Table S3) and repeated the genetic association analyses. For the PC derived traits, we identified eight diet-independent and one diet-dependent QTLs that were not identified in our analysis of the directly measured traits (Table 1).

We were able to map QTLs to narrow intervals containing one to dozens of genes because linkage disequilibrium was not extensive for these DO generations (22–28). Linkage disequilibrium for genotyped marker pairs at distances of 10–100 kb (i.e., the distance between the majority of mouse gene pairs) was less than 0.5 for the majority of chromosomes (Supplementary Figure S6). To more precisely fine-map the genomic interval of each QTL, we imputed all SNPs and small insertion-deletion variants from the fully sequenced DO founders (Keane et al. 2011) for a 5 Mb interval centered at the lead genotyped marker. For each imputed variant, we identified the founder-of-origin for the major and minor allele. To illustrate this process, consider a bi-allelic A/G variant. If

Table 1 Genome-wide significant diet-independent and diet-dependent QTLs

Physiological cluster		Trait ID	Chr	P-value	Founder allele pattern	FAP rank	FAP interval		FAP variants	Lead candidate genes
							Start	End		
Additive model	DEXA 1. bone comp.	PC_DXB1	5	<0.001	AJ/129/NZO/CAST AJ/NZO	1 2	40.676951 40.595906	40.676951 40.595906	1 32	Nkx3-2
		DX_BARE	5	<0.001	PWK/W/WSB NZO/CAST	1 3	39.447772 39.750054	43.024779 41.900135	27 13	Nkx3-2
		DX_BOMC	5	<0.001	AJ/129/NZO/CAST NZO/CAST	1 2	40.676951 39.750054	40.676951 42.220331	1 18	Nkx3-2
		DX_BOMC	7	0.037	B6/PWK/W/WSB NZO/PWK/W/WSB	3 1	39.930802 3.294757	40.255407 4.882952	4 3	Aurkc
		PC_DXB1	7	0.082	B6 B6	2 1	5.498836 5.498836	10.730083 10.730083	24 24	Aurkc
		PC_DXB2	17	0.006	B6/NOD NOD	1 2	31.61965 33.561611	36.794365 40.436409	7 119	Aurkc Ddr1
		PC_DXB1	17	0.033	B6/CAST B6/NZO/CAST/PWK	1 2	82.942619 83.173711	83.636544 83.270033	7 11	Pkdcc, Mta3
		PC_DXB2	X	0.005	B6/NZO/CAST/W/WSB NOD	2 1	69.780554 24.268712	73.330769 26.92124	10 60	Nlgn1
		DX_PFBT	3	0.034	NOD 129/CAST	1 1	48.783896 57.432344	51.885719 62.393524	25 15	— Muskl, Ugcg
		DX_TTIME	4	0.044	AJ AJ	1 1	58.295722 58.802827	60.267128 59.350524	6 23	Muskl, Ugcg Muskl, Ugcg
DX_SIZE	4	0.02	CAST NOD/NZO	2 1	110.460182 115.058995	114.693547 116.711414	3 5	Tph2		
DEXA 2. body comp.	PC_DXS2	10	0.016	B6/NOD/NZO AJ/CAST	2 1	111.32045 12.412183	112.084464 18.30634	22 43	Kcrnj16, Kcmj2	
	PC_DXS2	11	0.065	B6 B6	1 1	13.078266 12.999179	16.232304 15.791595	6 41	Lig1	
	DX_TARE	17	0.074	B6/NZO/PWK PWK	1 2	30.48983 29.86344	30.674742 31.955227	2 2	Nrg1	
	AS_XINF	7	0.089	129/NOD/PWK 129/NOD	2 2	55.66213 59.59402	65.634751 67.81307	441 354	Cdh23	
	AS_XINF	8	0.019	CAST/PWK/W/WSB CAST/PWK/W/WSB	1 1	59.59402 59.59402	67.938722 67.938722	355 6	Cdh23	
	AS_YINF	10	<0.001	AJ/PWK AJ	1 2	107.683859 106.702389	108.921283 107.189894	2 2	Pde4d	
	AS_TAUC	10	<0.001	129/NOD/NZO 129/NOD	1 1	4.026123 4.026123	9.375212 9.375212	15 15	Col1a2	
	PC_ACS1	10	<0.001	AJ/CAST 129/NOD/NZO	1 1	79.909399 36.709005	82.052705 38.111135	12 4	Col1a2 Ptprd	
	AS_SLOP	13	0.013	AJ/PWK NOD/NZO	1 2	38.25979 49.91309	39.03838 50.30859	5 2	Kcnn4	
	EC_LVPD	6	0.018	NZO B6/W/WSB	1 2	50.640198 58.502569	50.64876 60.484421	3 14	—	
ECHO 1. LV posterior wall thickness ECHO 4. cardiac output	EC_LVPD	6	0.018	NZO/CAST/W/WSB AJ/129/NZO	1 1	77.735404 39.026308	81.435051 47.936594	20 90	Ptprd	
	PC_ECL1	4	0.038	CAST/PWK B6/W/WSB	1 1	77.027818 77.027818	82.136588 82.136588	20 20	Trhr	
	PC_ECC3	4	0.038	CAST/PWK B6/W/WSB	1 1	31.005111 32.914841	34.784299 34.073575	31 18	Cttna2	
	PC_ECC2	18	0.045	B6/129/NZO AJ	1 1	34.986815 98.839327	38.326179 99.729097	18 38	Cttna2 Hmncn1, Lmx1b	
	EC_LVID	X	0.098	NZO/CAST/PWK NZO	1 1	98.839327 98.839327	99.729097 99.729097	38 38	Lmx1b Fstl1	
	WR_MDAY	18	0.051	— —	1 1	— —	— —	— —	— —	
	WR_MNIG	4	0.097	— —	1 1	— —	— —	— —	— —	
	PC_WRN2	15	0.017	— —	1 1	— —	— —	— —	— —	
	PC_ROR1	6	0.079	— —	1 1	— —	— —	— —	— —	
	RR_FIRS	6	0.069	— —	1 1	— —	— —	— —	— —	
Interaction	ECHO 1.	PC_ECL1	2	0.023	— —	1 1	— —	— —	— —	— —
	LV posterior wall thickness	EC_LVPD	2	0.027	— —	1 1	— —	— —	— —	— —
	ECHO 3.- ejection fraction	PC_ECE2	16	0.033	— —	1 1	— —	— —	— —	— —
	Hearing	AS_YINF	9	0.095	— —	1 1	— —	— —	— —	— —

Traits are organized by clusters identified in Figure 4. For each trait, we calculated a genome-wide significant LOD score threshold using a permutation analysis. We identified the FAP of the variant with the strongest LOD score, the genomic location of these variants, and the number of significant variants that comprise the lead FAP group. For loci in which the lead FAP is comprised of fewer than 10 variants, we also present results for the second ranked FAP. We list likely candidate genes based on the location of lead FAP variants and previously described gene effects in the Mouse Genome Informatics database.

allele A was specific to founders AJ, NZO, and PWK and allele G was specific to the other 5 founders, then we assigned A to be the minor allele and defined a FAP of AJ/NZO/PWK for this variant. Importantly, the FAP is a measure of identity-by-state for imputed SNPs, and contrasts with the founder-of-origin genotype probabilities that measures identity-by-descent in the DO population or the Strain Distribution Pattern developed for mouse recombinant inbred lines mapping populations (Dietrich *et al.* 1992).

To identify the variants and founder haplotypes most likely responsible for the association at each locus, we grouped variants based on their FAP and ranked groups based on the largest LOD score among its constituent variants. (Note that, by definition, no variant can be a member of more than one FAP group.) We hypothesized that the functional variant(s) responsible for trait-specific variation were among those in the lead FAP group because they exhibit the strongest statistical association and it is unlikely any additional variants are segregating in this genomic interval beyond those identified in the full genome sequences of the eight founder strains. By focusing on FAP groups with the largest LOD scores, we narrowed the number of candidate variants at each QTL. The lead FAP and the number and location of statistically significant variants that comprise each FAP group

are summarized in Table 1. In addition, a list of all imputed variants significantly associated with each trait and the candidate genes in each region are provided in Supplementary Files S3 and S4. To demonstrate this approach, we fine-mapped QTLs associated with bone composition traits.

Alleles of contrasting effects associated with variation in bone composition

Traits comprising the tightly correlated bone composition cluster (Figure 4) were associated with a chromosome 5 locus (total bone area and mineral content) and a chromosome 7 locus (bone mineral content, Figure 5A). It is unsurprising that the locus with the greatest LOD score, chromosome 5, was associated with both total bone area and bone mineral content because these two traits are both correlated with mouse size (Brommage 2003). We repeated the genetic association analysis with PC derived bone composition traits and found PC1 replicated the chromosome 5 association and the strength of the chromosome 7 association was reduced (Table 1). In addition, the PC1 analysis identified a new peak on chromosome 17 and PC2 analysis identified two new QTLs on chromosomes 17 and X (Figure 5B). To identify candidate variants and genes, we fine-mapped these loci using the FAP group of each imputed variant.

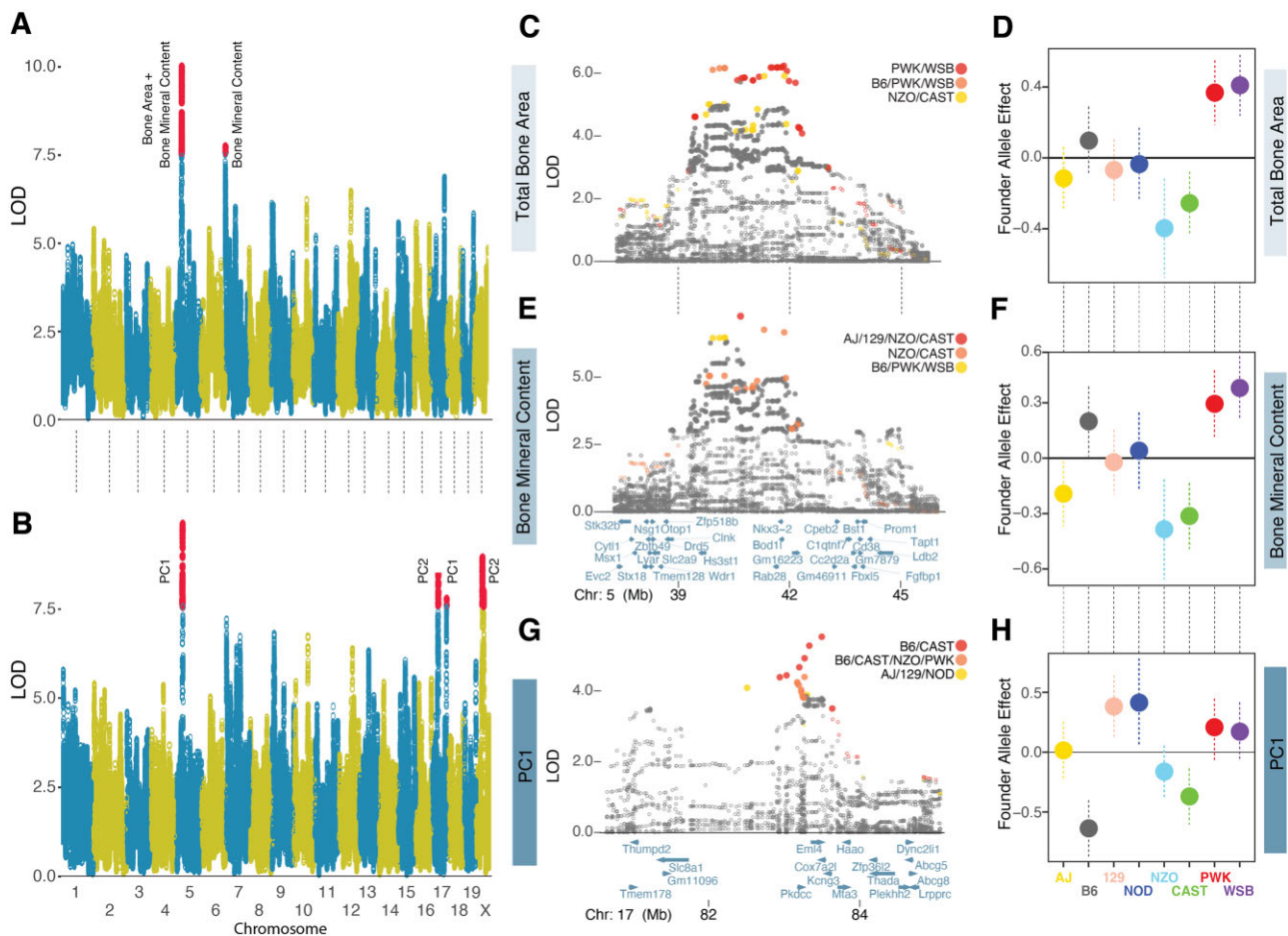


Figure 5 (A) Manhattan plot of directly measured bone composition traits: total bone area and bone mineral content. Red circles denote markers with statistically significant ($P < 0.05$) LOD score based on genome-wide permutation analysis. (B) Manhattan plot of PC derived bone physiology traits. (C) Fine mapping of total bone area (DX_BARE) chromosome 5 locus using imputed variants. LOD scores of closed circles are statistically significant ($P < 0.05$) based on permutation analysis of all imputed variants with ± 5 Mb of lead genotyped marker. Variants in three FAP groups shown in red, orange, and yellow circles, ordered by maximum LOD score. (D) Mean founder allele effect (\pm standard error) for the lead genotyped variant for total bone area (DX_BARE). Panels E and F are the same as C and D for bone mineral content (DX_BOMC). Panels G and H are the same as C and D for the chromosome 17 bone composition-PC1 (PC_DX_B1) locus.

We fine-mapped the chromosome 5 loci associated with total bone area (DX_BARE) and bone mineral content (DX_BOMC). The lead FAP for DX_BARE (ranked by maximum LOD score of each FAP variant group) contained variants with minor alleles specific to the PWK and WSB founders and the rank 2 FAP was very similar: it contained variants specific PWK, WSB, and B6 (Figure 5C). Given that our FAP definition means no variant can be a member of more than one FAP group, this result illustrates that the founder haplotypes were well mixed in this DO population and that multiple similar haplotypes are segregating at this locus. The high LOD scores for these similar FAPs suggested that the functional variant was likely derived from PWK and WSB and the elevated LOD score for the rank 2 FAP that included B6 was caused by tight LD between the rank 1 and 2 FAP groups. In contrast, the rank 3 FAP was comprised of a nonoverlapping set of founders: NZO and CAST (Figure 5C). The strong statistical association of these dissimilar FAP groups was because the PWK and WSB alleles were associated with the largest positive effect of the eight founders on total bone area, whereas NZO and CAST were associated with the largest negative effect (Figure 5D). Next, we examined the fine-mapping results for DX_BOMC and identified a different order of lead FAPs: rank 1 and 2 groups contained minor alleles specific to the NZO and CAST founders whereas the rank 3 group was comprised of PWK and WSB (Figure 5E). The effects of the founder alleles on bone mineral content (Figure 5F) were similar to results for total bone area (Figure 5D). Although the rank order of the top three FAP groups differed slightly between the two traits, these results are consistent with the hypothesis that this one locus affects these two highly similar traits. Moreover, we have identified at least three distinct alleles at this locus: a positive allele derived from the PWK and WSB founders, a negative allele derived from the NZO and CAST founders, and a neutral allele derived from the four other founders.

To further illustrate the utility of fine mapping QTLs with variants grouped by FAP, we examined the chromosome 17 locus associated with bone composition PC1 (Figure 5B). We found that variants with minor alleles specific to the B6 and CAST founders exhibited the strongest statistical association (Figure 5G). Consistent with the composition of this lead FAP, we found the effect of the B6 and CAST founder alleles to have the largest negative effects on bone composition PC1 (Figure 5H).

We identified candidate genes at these QTLs by intersecting the position of lead FAP grouped variants and previously described gene effects in the Mouse Genome Informatics database (www.informatics.jax.org). The chromosome 5 total bone area QTL contained 406 significant variants, of which 27 (21 intergenic SNPs, 6 intronic SNPs) were specific to the positive effect PWK/WSB alleles (rank 1 FAP group) and 13 (12 intergenic SNPs and 1 intronic SNP) were specific to the negative effect NZO/CAST alleles (rank 3 FAP group; Table 1, Figure 5C). The chromosome 5 bone mineral content QTL contained 350 significant variants, of which 4 intergenic SNPs were specific to the positive B6/PWK/WSB alleles (rank 3 FAP group) and 19 (17 intergenic SNPs and 2 intronic SNPs) were specific to the negative effect NZO/CAST alleles (rank 1 and 2 FAP groups; Figure 5E). We found no protein-coding variants in the lead FAP groups that were significantly associated with either trait, suggesting that the functional variant(s) altered gene expression. All candidate variants were intergenic or intronic SNPs located in a genomic interval containing five genes: *Hs3st1*, *Rab28*, *Nkx3-2*, *Bod1l*, and *Gm16223* (Figure 5, C and E, Supplementary Files S3 and S4). Of these candidates *Nkx3-2* encodes a homeobox protein previously shown to affect skeleton development (Lettice et al. 1999). The

chromosome 17 locus associated with bone composition PC1 was comprised of 47 statistically significant variants, seven of which were members of the B6/CAST FAP (Figure 5G). All of these variants were intergenic SNPs located in a genomic interval containing five genes: *Pkdcc*, *Eml4*, *Cox7a21*, *Kcng3*, and *Mta3* (Supplementary Files S3 and S4). Of these candidates *Pkdcc* has previously been shown to effect bone morphology (Imuta et al. 2009; Sajan et al. 2019).

These analyses illustrate three key findings: (1) conducting genetic association analyses with both directly measured and PC derived traits can reveal novel loci, (2) fine mapping loci with FAP groups greatly reduces the number of lead candidate variants, and (3) FAP variant groups illuminate the link between specific founder haplotypes associated with positive, neutral, or negative phenotypic effects.

Cardiac physiology is altered in response to dietary intervention in a genotype-dependent manner

All three significant diet-dependent QTLs were associated with cardiac physiology traits (Table 1). We identified one QTL associated with the second PC (PC2_ECE2) of ejection fraction (EC_EFRA) and left ventricular inner dimension, systole (EC_LVIS) (Figure 6A). These two traits are positively correlated with PC2_ECE2 (Supplementary Figure S7), which we interpreted as a measure of heart pumping efficiency. We fine-mapped this QTL and found the lead FAP was composed of AJ-specific alleles (Figure 6A). In order to determine the diet most likely responsible for the significant GxD interaction effects, we compared the lead variant LOD score in the full model to reduced models in which we pruned diets in singles and pairs. We considered a diet as likely responsible for the significant interaction effect if the removal of that diet reduced the strength of the association in comparison to the full model. For PC_ECE2, we found that 20% CR and 2D fast treatments were most likely responsible for the diet-dependent association (Supplementary Table S4). The diet-specific founder-allele effect for the AJ allele exhibited the largest positive effects in the 20% CR and 2D fast treatments and significant negative effects in AL and 40% CR treatments (Figure 6B). These results are consistent with the hypothesis that the diet-dependent effects of the AJ allele were responsible for the interaction association at this locus. We identified 18 variants significantly associated with PC_ECE2 and all of these were specific to the lead FAP, AJ. A single variant was an intergenic structural variant, and the remaining 17 were noncoding exonic (1), intronic (4) or intergenic (12) located at nine genes (Supplementary Files S3 and S4). One variant was located in the 3' UTR of *Fstl1*, which is a secreted glycoprotein expressed in the adult heart that affects cardiac morphology, contractility, and vascularization (Oshima et al. 2008; Shimano et al. 2011).

The remaining diet-dependent QTLs were associated with diastolic left ventricular posterior wall thickness (EC_LVPD) and the first principal component (PC_ECL1) of EC_LVPD and EC_LVPS, systolic left ventricular posterior wall thickness (Table 1). EC_LVPD and EC_LVPS are positively correlated (Figure 4A) and, unsurprisingly, the QTLs for PC_ECL1 and EC_LVPD were located in the same region of chromosome 2 and shared the same lead FAP: B6/129/NZO (Figure 7, A and B). We found the genomic interval associated with PC_ECL1 to be larger than EC_LVPD (30.9–34.8 Mb vs 32.9–34.1 Mb) and fine-mapping EC_LVPS revealed a region of association between 30.5 and 32.0 Mb (Supplementary Figure S8). Although the size of our mapping population and the extent of LD (Supplementary Figure S6) limits our ability to conclude whether the associations

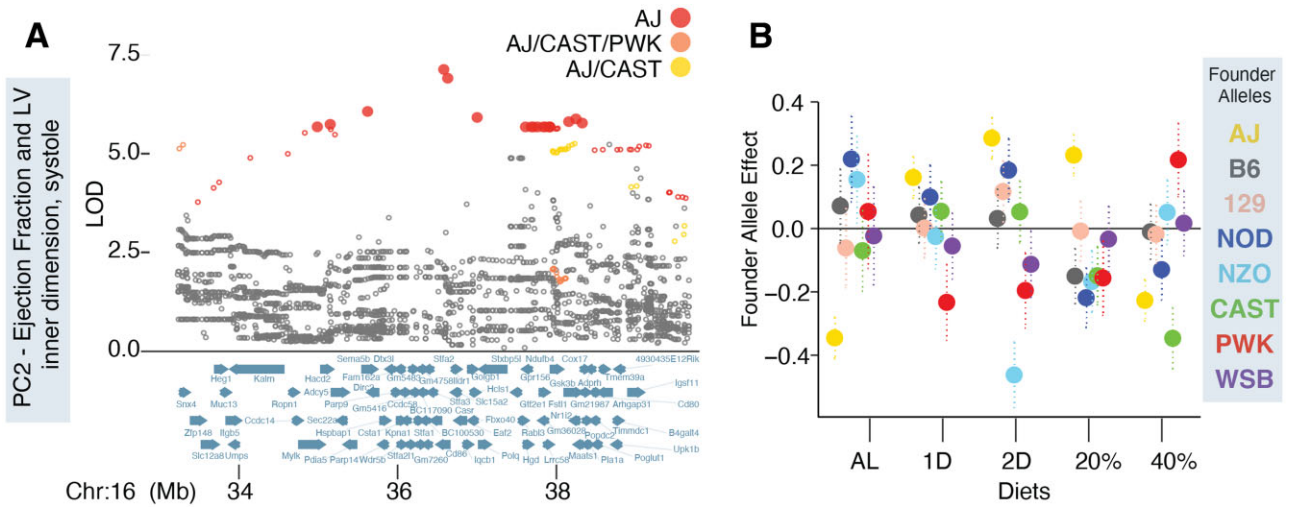


Figure 6 (A) Fine mapping of chromosome 16 locus associated with PC2 of ejection fraction and left ventricular inner dimension, systole (PC_ECE2). Rank 1, 2, and 3 FAP variants shown in red, orange, and yellow circles. LOD scores of closed circles are statistically significant ($P < 0.05$) based on permutation analysis of all imputed variants with ± 5 Mb of lead genotyped variant. (B) Mean diet-specific founder allele effects (\pm standard error) for the lead genotyped variant for PC_ECE2.

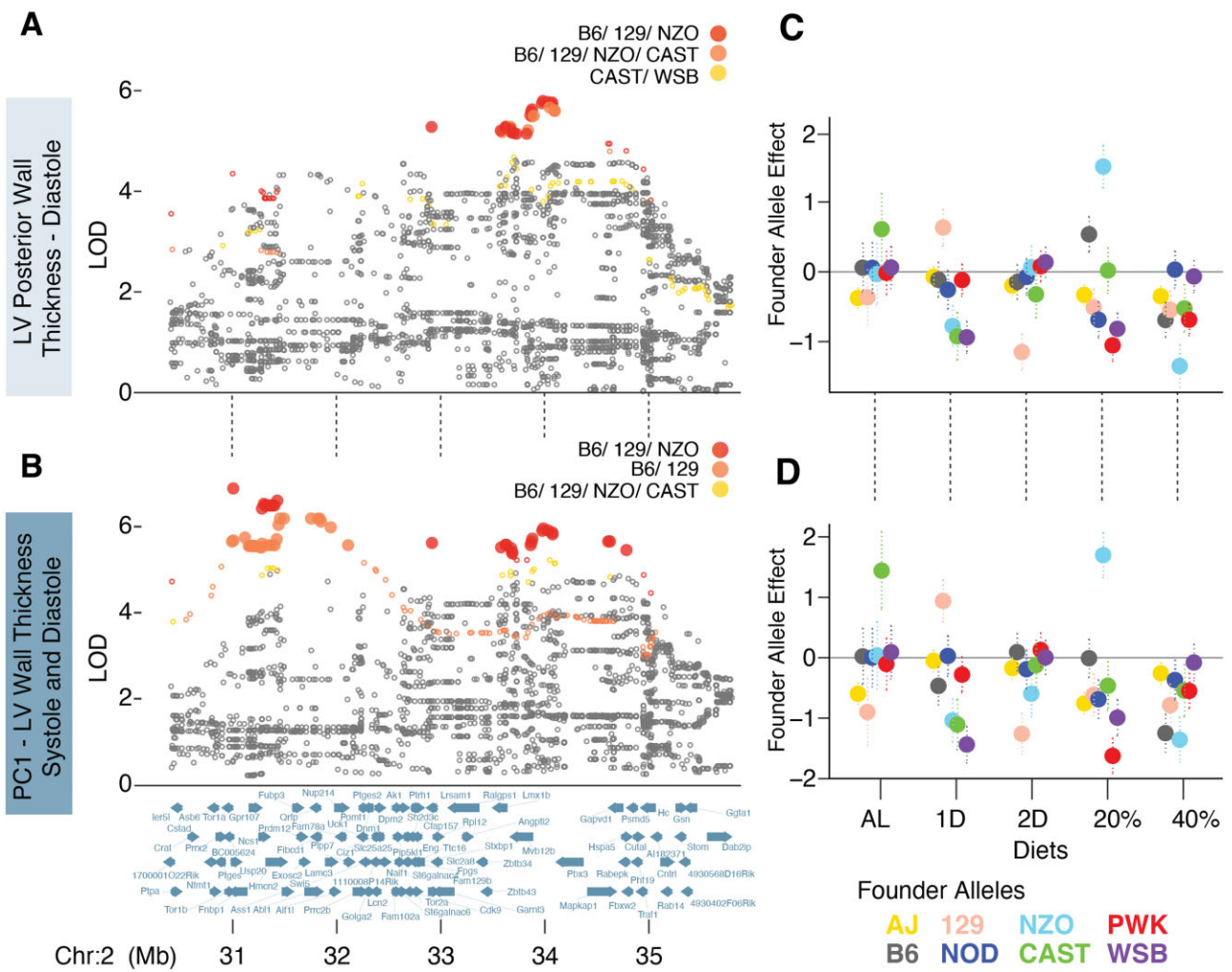


Figure 7 (A) Fine mapping of chromosome 2 locus associated with left ventricular posterior wall thickness, diastole (EC_LVPD). Rank 1, 2, and 3 FAP variants shown in red, orange, and yellow circles. LOD scores of closed circles are statistically significant ($P < 0.05$) based on permutation analysis of all imputed variants with ± 5 Mb of lead genotyped marker. (B) Fine mapping of chromosome 2 locus associated with PC1 of left ventricular posterior wall thickness, systole and diastole (PC_ECL1), details are the same as in A. Mean diet-specific founder allele effects (\pm standard error) for the lead genotyped variant for EC_LVPD (C) and PC_ECL1 (D).

with systolic and diastolic wall thickness are separate loci affected by distinct functional variants, this result does explain the subtle difference between the fine mapped intervals for PC_ECL1 and EC_LVPD (Figure 7, A and B). We next set out to determine which dietary intervention(s) were responsible for these genotype-by-diet interaction effects.

Using the reduced GxD association model test, we found the 20% CR and 1D fast treatments were most likely responsible for the diet-dependent associations with EC_LVPD and PC_ECL1 (Supplementary Table S4). We estimated the diet-specific founder-allele effects for the lead variant at this QTL and focused on the effects of B6, 129 and NZO. We estimated distinct diet-specific effects for each founder: the effect of B6 was significantly negative in 40% CR, positive in 20% CR (for EC_LVPD only), and largely neutral in the other three diets; the effect of 129 was significantly positive in the 1D fast treatment and negative in the other four diets; the effect of NZO was significantly positive in 20% CR, neutral in AL, and negative in the other three diets (Figure 7, C and D). Although the B6 allele was identified in the lead FAP, the effect size results suggest this allele was unlikely to be responsible for the GxD interaction association. The seeming incongruence between the FAP and effect-size estimates illustrates a key point: FAPs were annotated using imputed variants and reflect identity-by-state whereas effect-sizes were estimated using the founder-of-origin probabilities and reflect identity-by-descent (as described in Methods section). These results were consistent with the hypothesis that either 129 or NZO founder alleles were responsible for the significant interaction QTL because of the strong diet-specific effect of the 129 allele in 1D fast and NZO allele in 20% CR. In addition, these results would be consistent with the hypothesis that both founder alleles are responsible and, given our observation of contrasting diet-specific effects, each may harbor distinct functional variants at this QTL.

We identified a total of 59 and 28 variants significantly associated with PC_ECL1 and EC_LVPD. Thirty-one PC_ECL1 variants and 18 EC_LVPD variants were specific to the lead FAP (B6/129/NZO) and all variants were SNPs. Variants associated with PC_ECL1 (19 intronic and 12 intergenic) were located in close proximity to 10 genes (Supplementary Files S3 and S4). Ten variants (eight intronic and two immediately upstream) were located at *Hemicentin2*, a fibulin family extracellular matrix protein. Genetic knock-out studies of *Hmcn2* have resulted in abnormal left ventricular morphology in mice (Dickinson et al. 2016) and have been associated with electrocardiogram-derived traits in humans (Tereshchenko et al. 2018). In addition, three variants (intronic) were located at *Lmx1b*, a LIM homeobox transcription factor 1-beta that is known to regulate limb and organ development (Dreyer et al. 1998; Schweizer et al. 2004; Doucet-Beaupré et al. 2016). Variants associated with EC_LVPD (9 intronic and 9 intergenic) were located in close proximity to 5 genes, a list which included *Lmx1b* and lacked *Hmcn2* (Supplementary Files S3 and S4).

Taken together, all significant diet-dependent QTLs were associated with heart physiology. Fine mapping with FAPs narrowed the likely number of causal variants and identified candidate genes previously linked to cardiac morphology or function. We previously showed that the signs of the effects of diet on the mean physiological trait measurements were specific to the type of intervention (CR or IF) and their magnitudes were nonadditive with respect to the magnitude of intervention (Figure 2). Identification of candidate genes with diet-dependent effects suggests molecular mechanisms to explain these results.

Discussion

Conditionally beneficial effects of CR and IF on distinct aspects of physiology

A primary goal of this study was to address the question: which aspects of physiology would respond to dietary intervention in adult mice? We performed this experiment using DO mice in order to assess this question in an outbred genetic model that more closely resembles human populations. In addition, we were interested in determining whether the physiological health benefits (or detriments) of daily CR could be replicated with IF treatments. We found dietary intervention initiated at 6 months of age significantly altered many traits in 12-month-old mice. The 40% CR dietary intervention impacted the greatest number of traits in comparison to the AL diet followed by the 20% CR, 2D and 1D fast treatments (Figure 2). Using six experimental assays we clustered individual traits into distinct aspects of physiology (Figure 4). In many instances, changes to an aspect of physiology were not consistent between IF and CR. For the body composition cluster, we observed similar reductions in mean body weight for the 20% CR and 2D fast treatments in comparison to AL, however the 2D fast treatment increased the percentage of fat mass, whereas the 20% CR decreased the percentage of fat mass (Figure 2). How might these changes in physiology impact organismal health?

While the lifespan extension of daily CR is well established, it remains largely unknown whether dietary intervention would improve physiological function in healthy, adult mice. Our results demonstrated that 40% CR improved multiple aspects of cardiovascular function. The 40% CR treatment significantly reduced left ventricular posterior wall thickness in diastole and trended toward a significant reduction in systole (Figure 2). In addition, 40% CR mice had increased ejection fraction and increased stroke volume after controlling for their decreased body weight (Supplementary Figure S2). All three of these trends: reduced posterior wall thickness, increased ejection fraction, and increased stroke volume are associated with younger mice and improved cardiac health outcomes (Mattson and Wan 2005; Medrano et al. 2016; Lindsey et al. 2018). In contrast, the 20% CR treatment caused a significant reduction in ejection fraction and stroke volume (Figure 2), regardless of body weight correction (Supplementary Figure S2), which is indicative of poor cardiac health. However, the 20% CR treatment was not universally detrimental because it also caused a significant beneficial decrease in systolic and diastolic left ventricular posterior wall thickness. Interestingly, the 2D fast treatment produced nearly opposite results to 20% CR: we observed a beneficial increase in ejection fraction and stroke volume and a detrimental increase in left ventricular posterior wall thickness (systolic and diastolic). Although these results were not statistically significantly different from AL (Figure 2), they suggested 2D fast improved some aspects of cardiac health and degrades others in a manner opposite to the 20% CR treatment. These results highlight the complex manner in which the type and magnitude of dietary intervention may improve or degrade cardiac health and may explain the seemingly contradictory results of IF and CR interventions observed in other rodent models (Ahmet et al. 2005, 2011).

We examined the effect of dietary intervention on other aspects of physiological health and found that the 40% CR treatment was not universally beneficial. The 40% CR group had the lowest hearing ability across the entire auditory range tested, whereas hearing ability was greatest in the AL group (Figure 2). These results contradict previous studies that found CR prevented age-related hearing loss (Someya et al. 2007 2010). Similar

to hearing ability, we observed bone mineral density was lowest in 40% CR and greatest in AL diet (DX_BOMD; Figure 2). These results were consistent with human clinical trial which showed cardiovascular function was improved and bone mineral density was degraded following a 25% CR intervention (Villareal et al. 2006, 2016; Kraus et al. 2019). By measuring multiple aspects of physiology in a large outbred mouse population, we identified contrasting effects of CR and IF on health. With continued observation, we will determine whether the year one effects will have lasting physiological effects on health and explain the physiological mechanisms by which dietary intervention extends lifespan.

The effect of select genetic variants on physiological health may be as impactful as dietary intervention

The majority of traits (31 of 36) derived from six phenotypic assays exhibited significant genetic heritabilities (Figure 3). Genetic mapping analyses with directly measured and PC derived traits identified both diet-independent and diet-dependent QTLs associated with distinct aspects of physiology (Table 1). We found the effect of founder alleles at some QTLs were as strong or stronger than the effect of dietary intervention. For instance, the difference between positive and negative founder-allele-effects for the lead genotyped variant at the chromosome 5 bone mineral content QTL (0.77, Figure 5F) exceeded the negative effect of 40% CR diet (−0.57). This suggested that the potentially detrimental effect of 40% CR on bone mineral content may be offset by the beneficial effect of the PWK and WSB founder alleles. Similarly, the negative effect of 40% CR on hearing ability (−0.31) could be offset by the significantly positive effect of the WSB, PWK, CAST alleles (1.19) at the chromosome 10 QTL (Table 1). One caveat to this interpretation is that some variation observed within the daily CR treatments may be due to variable caloric intake because mice were group housed and individual feeding behavior could not be controlled.

The candidate genes at these loci maybe fruitful targets for genetic manipulation or therapeutic intervention to either mimic beneficial or ameliorate detrimental effects of CR and IF. While mapping resolution in the DO is much better than in classical mouse crosses (Supplementary Figure S6), and it is further improved by the ancestral genotype states in the FAP analysis, the typical QTL region in this analysis contains one to dozens of genes. Our approach has been to use functional information, when available, to prioritize candidates but we cannot rule out other genes or functional elements within the QTL region. Finally, the extensive genetic correlations identified between traits, both within and between clusters, suggests that interventions may have pleiotropic effects (perhaps positive or negative) beyond the focal trait.

No clear overlap with other QTL mapping results

We found no overlapping QTLs for similar traits between this study and those identified in four other Diversity Outcross mouse studies (Svenson et al. 2012; Tyler et al. 2017; Katz et al. 2020; Al-Barghouthi et al. 2021) and one high resolution mapping study in outbred CFW mice (Parker et al. 2016). At least three factors may contribute to the paucity of overlapping QTLs: (1) there are relatively few DO or other high resolution mouse QTL studies that have measured similar traits, (2) some QTLs with significant trait effects may not be detected in a single experiment (due to the Beavis effect), therefore the likelihood of detecting overlapping QTLs when comparing between experiments is reduced, and (3) age, sex and dietary treatments vary between studies and specific QTL effects may be dependent upon these factors (Wright et al. 2020).

Cardiac morphology and function is shaped by diet-dependent genetic associations

Cardiac morphology and function were the only physiological traits for which we identified significant diet-dependent QTLs. Variation in cardiac pumping efficiency, quantified with PC_ECE2, was associated with an AJ specific allele that increased function in 20% CR, 1D, and 2D fast treatments and decreased function in the AL and 40% CR treatments (Figure 6D). Interestingly, the diet-dependent effect of the NZO allele at this locus was nearly opposite that of AJ and the difference between these alleles in the AL (0.500) and 2D fast (0.746) treatments was of similar magnitude of the difference between diets (0.631). We highlight this example to illustrate that the beneficial or detrimental effects of diet maybe ameliorated by genetic variants segregating within the DO mouse population. These results provide additional support for the hypothesis that cardiac efficiency maybe altered to the same degree as CR or IF with genetic manipulation or therapeutic intervention to phenocopy the AJ or NZO allele. In addition, the large diet-specific effects of the 129 and NZO alleles (Figure 6, E and F) suggest that similar approach could be utilized to manipulate LV posterior wall thickness. The decline in cardiac health in response to diet and age is a leading risk factor for reduced lifespan in human populations (Dwyer-Lindgren et al. 2016). These results clearly demonstrate that functional variants are segregating within the DO population to modulate cardiac morphology and function in a diet-specific manner and suggest possible interventions to protect against the diet-induced or age-related decline of cardiac health.

Future considerations and limitations

In summary, we found that multiple aspects of physiology in adult mice change in response to dietary intervention. Using a diverse set of experimental assays, we identified dietary interventions that may improve or degrade health along multiple axes of physiology. It is unknown how changes observed at 1 year of age, after 6 months of treatment, will impact health at later ages. As these mice age, we will continue to monitor them with the ultimate goal of identifying the physiological mechanisms by which dietary interventions improve or deteriorate health at advanced age.

Data availability

The raw genotype data, eight-state founder allele probabilities calculated in the qtl2 R package, and z-score transformed phenotypic data used for all analyses are available on figshare: <https://doi.org/10.25386/genetics.15060894>. Supplementary Files S1–S4 are also available in the same figshare deposit.

Acknowledgments

The authors would like to acknowledge Natalie Telis, J. Graham Ruby, Nick van Bruggen and David Botstein for their comments on the manuscript. Funding was provided by Calico Life Sciences LLC.

Conflicts of interest

Authors Guozhu Zhang, Anil Raj, Baby Martin-McNulty, Ganesh A. Kolumam, Johannes Riegler, Adam Freund, and Kevin M. Wright are employees of Calico Life Sciences LLC.

Literature cited

- Ahmet I, Tae HJ, de Cabo R, Lakatta EG, Talan MI. 2011. Effects of caloric restriction on cardioprotection and cardiovascular health. *J Mol Cell Cardiol.* 51:263–271.
- Ahmet I, Wan R, Mattson MP, Lakatta EG, Talan M. 2005. Cardioprotection by intermittent fasting in rats. *Circulation.* 112:3115–3121.
- Al-Barghouthi BM, Mesner LD, Calabrese GM, Brooks D, Tommasini SM, et al. 2021. Systems genetics in diversity outbred mice inform BMD GWAS and identify determinants of bone strength. *Nat Commun.* 12:3408.
- Anton SD, Moehl K, Donahoo WT, Marosi K, Lee SA, et al. 2018. Flipping the Metabolic Switch: Understanding and Applying the Health Benefits of Fasting. *Obesity.* 26:254–268.
- Bauer M, Hamm AC, Bonaus M, Jacob A, Jaekel J, et al. 2004. Starvation response in mouse liver shows strong correlation with life-span-prolonging processes. *Physiol Genomics.* 17:230–244.
- Benjamini Y, Hochberg Y. 1995. Controlling the false discovery rate: a practical and powerful approach to multiple testing. *J R Statist Soc B (Methodological).* 57:289–300.
- Broman KW, Gatti DM, Simecek P, Furlotte NA, Prins P, et al. 2019. R/qtl2: software for mapping quantitative trait loci with high-dimensional data and multiparent populations. *Genetics.* 211:495–502.
- Brommage R. 2003. Validation and calibration of DEXA body composition in mice. *Am J Physiol Endocrinol Metab.* 285:E454–E459.
- Bruss MD, Khambatta CF, Ruby MA, Aggarwal I, Hellerstein MK. 2010. Calorie restriction increases fatty acid synthesis and whole body fat oxidation rates. *Am J Physiol.* 298:108–116.
- Cao SX, Dhahbi JM, Mote PL, Spindler SR. 2001. Genomic profiling of short- and long-term caloric restriction effects in the liver of aging mice. *Proc Natl Acad Sci USA.* 98:10630–10635.
- Carpenter B, Gelman A, Hoffman MD, Lee D, Goodrich B, et al. 2017. Stan: a probabilistic programming language. *J StatSoftw.* 76:1–32. doi:10.18637/jss.v076.i01.
- Churchill GA, Doerge RW. 1994. Empirical threshold values for quantitative trait mapping. *Genetics.* 138:963–971.
- Churchill GA, Gatti DM, Munger SC, Svenson KL. 2012. The diversity outbred mouse population. *Mamm Genome.* 23:713–718.
- Colman RJ, Anderson RM, Johnson SC, Kastman EK, Kosmatka KJ, et al. 2009. Caloric restriction delays disease onset and mortality in rhesus monkeys. *Science.* 325:201–204.
- Commo F, Bot BM. 2016. N-Parameter Logistic Regression [R package nplr version 0.1-7]. <https://github.com/fredcommo/nplr>. Last accessed Oct 26, 2021.
- Crawley JN. 2007. *What's Wrong with My Mouse?* Hoboken, NJ: John Wiley & Sons, Inc.
- Dhahbi JM, Kim HJ, Mote PL, Beaver RJ, Spindler SR. 2004. Temporal linkage between the phenotypic and genomic responses to caloric restriction. *Proc Natl Acad Sci USA.* 101:5524–5529.
- Dickinson ME, Flenniken AM, Ji X, Teboul L, Wong MD, et al.; RIKEN BioResource Center. 2016. High-throughput discovery of novel developmental phenotypes. *Nature.* 537:508–514.
- Dietrich W, Katz H, Lincoln SE, Shin HS, Friedman J, et al. 1992. A genetic map of the mouse suitable for typing intraspecific crosses. *Genetics.* 131:423–447.
- Doucet-Beaupré H, Gilbert C, Profes MS, Chabrat A, Pacelli C, et al. 2016. Lmx1a and Lmx1b regulate mitochondrial functions and survival of adult midbrain dopaminergic neurons. *Proc Natl Acad Sci USA.* 113:E4387–E4396.
- Dreyer SD, Zhou G, Baldini A, Winterpacht A, Zabel B, et al. 1998. Mutations in LMX1B cause abnormal skeletal patterning and renal dysplasia in nail patella syndrome. *Nat Genet.* 19:47–50.
- Dwyer-Lindgren L, Bertozzi-Villa A, Stubbs RW, Morozoff C, Kutz MJ, et al. 2016. US County-level trends in mortality rates for major causes of death, 1980–2014. *JAMA.* 316:2385–2401.
- Escabi CD, Frye MD, Trevino M, Lobarinas E. 2019. The rat animal model for noise-induced hearing loss. *J Acoust Soc Am.* 146:3692–3709.
- Furlotte NA, Eskin E. 2015. Efficient multiple-trait association and estimation of genetic correlation using the matrix-variate linear mixed model. *Genetics.* 200:59–68.
- Gatti DM, Svenson KL, Shabalin A, Wu LY, Valdar WW, et al. 2014. Quantitative trait locus mapping methods for diversity outbred mice. *G3 (Bethesda).* 4:1623–1633.
- Gelman A, Rubin DB. 1992. Inference from iterative simulation using multiple sequences. *Stat Sci.* 7:457–472.
- Goodrick CL, Ingram DK, Reynolds MA, Freeman JR, Cider N. 1990. Effects of intermittent feeding upon body weight and lifespan in inbred mice: interaction of genotype and age. *Mech Ageing Dev.* 55:69–87.
- Gräff J, Kahn M, Samiei A, Gao J, Ota KT, et al. 2013. A dietary regimen of caloric restriction or pharmacological activation of SIRT1 to delay the onset of neurodegeneration. *J Neurosci.* 33:8951–8960.
- Gredilla R, Barja G. 2005. The role of oxidative stress in relation to caloric restriction and longevity. *Endocrinology.* 146:3713–3717.
- Gulinello M, Mitchell HA, Chang Q, Timothy O'Brien W, Zhou Z, et al. 2019. Rigor and reproducibility in rodent behavioral research. *Neurobiol Learn Mem.* 165:106780.
- Halagappa VKM, Guo Z, Pearson M, Matsuoka Y, Cutler RG, et al. 2007. Intermittent fasting and caloric restriction ameliorate age-related behavioral deficits in the triple-transgenic mouse model of Alzheimer's disease. *Neurobiol Dis.* 26:212–220.
- Harper JM, Leathers CW, Austad SN. 2006. Does caloric restriction extend life in wild mice? *Aging Cell.* 5:441–449.
- Heilbronn LK, Ravussin E. 2003. Calorie restriction and aging: review of the literature and implications for studies in humans. *Am J Clin Nutr.* 78:361–369.
- Imuta Y, Nishioka N, Kiyonari H, Sasaki H. 2009. Short limbs, cleft palate, and delayed formation of flat proliferative chondrocytes in mice with targeted disruption of a putative protein kinase gene, Pkdcc (AW548124). *Dev Dyn.* 238:210–222.
- Kaerberlein M, Powers RW, Steffen KK, Westman EA, Hu D, et al. 2005. Cell biology: regulation of yeast replicative life span by TOR and Sch9 response to nutrients. *Science.* 310:1193–1196.
- Kafkafi N, Agassi J, Chesler EJ, Crabbe JC, Crusio WE, et al. 2018. Reproducibility and replicability of rodent phenotyping in pre-clinical studies. *Neurosci Biobehav Rev.* 87:218–232.
- Kang HM, Zaitlen NA, Wade CM, Kirby A, Heckerman D, et al. 2008. Efficient control of population structure in model organism association mapping. *Genetics.* 178:1709–1723.
- Katz DC, Aponte JD, Liu W, Green RM, Mayeux JM, et al. 2020. Facial shape and allometry quantitative trait locus intervals in the Diversity Outbred mouse are enriched for known skeletal and facial development genes. *PLoS One.* 15:e0233377.
- Keane TM, Goodstadt L, Danecek P, White MA, Wong K, et al. 2011. Mouse genomic variation and its effect on phenotypes and gene regulation. *Nature.* 477:289–294.

- Kim JU, Lee HJ, Kang HH, Shin JW, Ku SW, et al. 2005. Protective effect of isoflurane anesthesia on noise-induced hearing loss in mice. *Laryngoscope*. 115:1996–1999.
- Kraus WE, Bhapkar M, Huffman KM, Pieper CF, Das SK, et al. 2019. 2 years of calorie restriction and cardiometabolic risk (CALERIE): exploratory outcomes of a multicentre, phase 2, randomised controlled trial. *Lancet Diabetes Endocrinol*. 7:673–683.
- Lettice LA, Purdie LA, Carlson GJ, Kilanowski F, Dorin J, et al. 1999. The mouse bagpipe gene controls development of axial skeleton, skull, and spleen. *Proc Natl Acad Sci USA*. 96:9695–9700.
- Liang Y, Liu C, Lu M, Dong Q, Wang Z, et al. 2018. Calorie restriction is the most reasonable anti-ageing intervention: a meta-analysis of survival curves. *Sci Rep*. 8:5779.
- Liao CY, Rikke BA, Johnson TE, Diaz V, Nelson JF. 2010. Genetic variation in the murine lifespan response to dietary restriction: from life extension to life shortening. *Aging Cell*. 9:92–95.
- Lincoln SE, Lander ES. 1992. Systematic detection of errors in genetic linkage data. *Genomics*. 14:604–610.
- Lindsey ML, Kassiri Z, Virag JA, De Castro Brás LE, Scherrer-Crosbie M. 2018. Guidelines for measuring cardiac physiology in mice. *Am J Physiol Heart Circ Physiol*. 314:H733–H752.
- Mandillo S, Tucci V, Hölter SM, Meziane H, Al Banchaouchi M, et al. 2008. Reliability, robustness, and reproducibility in mouse behavioral phenotyping: a cross-laboratory study. *Physiol Genomics*. 34:243–255.
- Mattison JA, Colman RJ, Beasley TM, Allison DB, Kemnitz JW, et al. 2017. Caloric restriction improves health and survival of rhesus monkeys. *Nat Commun*. 8:14063.
- Mattson MP, Wan R. 2005. Beneficial effects of intermittent fasting and caloric restriction on the cardiovascular and cerebrovascular systems. *J Nutr Biochem*. 16:129–137.
- Maurissen JP, Marable BR, Andrus AK, Stebbins KE. 2003. Factors affecting grip strength testing. *Neurotoxicol Teratol*. 25:543–553.
- Medrano G, Hermosillo-Rodriguez J, Pham T, Granillo A, Hartley CJ, et al. 2016. Left atrial volume and pulmonary artery diameter are noninvasive measures of age-related diastolic dysfunction in mice. *J Gerontol Biol Sci Med Sci*. 71:1141–1150.
- Mitchell SJ, Madrigal-Matute J, Scheibye-Knudsen M, Fang E, Aon M, et al. 2016. Effects of sex, strain, and energy intake on hallmarks of aging in mice. *Cell Metab*. 23:1093–1112.
- Morgan AP, Fu CP, Kao CY, Welsh CE, Didion JP, et al. 2015. The mouse universal genotyping array: From substrains to subspecies. *G3 (Bethesda)*. 6:263–279.
- Mulligan JD, Stewart AM, Saupé KW. 2008. Downregulation of plasma insulin levels and hepatic PPAR γ expression during the first week of caloric restriction in mice. *Exp Gerontol*. 43:146–153.
- Oreper D, Cai Y, Tarantino LM, de Villena FPM, Valdar W. 2017. Inbred Strain Variant Database (ISVdb): a repository for probabilistically informed sequence differences among the collaborative cross strains and their founders. *G3 (Bethesda)*. 7:1623–1630.
- Oshima Y, Ouchi N, Sato K, Izumiya Y, Pimentel DR, et al. 2008. Follistatin-like 1 is an Akt-regulated cardioprotective factor that is secreted by the heart. *Circulation*. 117:3099–3108.
- Parker CC, Gopalakrishnan S, Carbonetto P, Gonzales NM, Leung E, et al. 2016. Genome-wide association study of behavioral, physiological and gene expression traits in outbred CFW mice. *Nat Genet*. 48:919–926.
- Patel NV, Gordon MN, Connor KE, Good RA, Engelman RW, et al. 2005. Caloric restriction attenuates A β -deposition in Alzheimer transgenic models. *Neurobiol Aging*. 26:995–1000.
- Pifferi F, Terrien J, Perret M, Epelbaum J, Blanc S, et al. 2019. Promoting healthspan and lifespan with caloric restriction in primates. *Nat Commun*. 2:1–3.
- Redman LM, Smith SR, Burton JH, Martin CK, Il'yasova D, et al. 2018. Metabolic slowing and reduced oxidative damage with sustained caloric restriction support the rate of living and oxidative damage theories of aging. *Cell Metab*. 27:805–815.e4.
- Sajan SA, Ganesh J, Shinde DN, Powis Z, Scarano MI, et al. 2019. Biallelic disruption of PKDCC is associated with a skeletal disorder characterised by rhizomelic shortening of extremities and dysmorphic features. *J Med Genet*. 56:850–854.
- Schweizer H, Johnson RL, Brand-Saber B. 2004. Characterization of migration behavior of myogenic precursor cells in the limb bud with respect to Lmx1b expression. *Anat Embryol (Berl)*. 208:7–18.
- Shimano M, Ouchi N, Nakamura K, Van Wijk B, Ohashi K, et al. 2011. Cardiac myocyte follistatin-like 1 functions to attenuate hypertrophy following pressure overload. *Proc Natl Acad Sci USA*. 108:E899–E906.
- Someya S, Yamasoba T, Weindruch R, Prolla TA, Tanokura M. 2007. Caloric restriction suppresses apoptotic cell death in the mammalian cochlea and leads to prevention of presbycusis. *Neurobiol Aging*. 28:1613–1622.
- Someya S, Yu W, Hallows WC, Xu J, Vann JM, et al. 2010. Sirt3 mediates reduction of oxidative damage and prevention of age-related hearing loss under Caloric Restriction. *Cell*. 143:802–812.
- Stan Development Team. 2020. RStan: The R Interface to Stan. R package version 2.21.2.
- Svenson KL, Gatti DM, Valdar W, Welsh CE, Cheng R, et al. 2012. High-resolution genetic mapping using the mouse. *Genetics*. 190:437–447.
- Tereshchenko LG, Sotoodehnia N, Sitlani CM, Ashar FN, Kabir M, et al. 2018. Genome-Wide associations of global electrical heterogeneity ECG phenotype: the ARIC (Atherosclerosis Risk in Communities) study and CHS (Cardiovascular Health Study). *J Am Heart Assoc*. 7:e008160.
- Tukey JW. 1977. *Exploratory Data Analysis*. 17th ed. Reading, MA: Addison-Wesley Pub. Co.
- Tyler AL, Ji B, Gatti DM, Munger SC, Churchill GA, et al. 2017. Epistatic networks jointly influence phenotypes related to metabolic disease and gene expression in diversity outbred mice. *Genetics*. 206:621–639.
- Villareal DT, Fontana L, Das SK, Redman L, Smith SR, et al.; for the CALERIE Study Group. 2016. Effect of two-year caloric restriction on bone metabolism and bone mineral density in non-obese younger adults: a randomized clinical trial. *J Bone Miner Res*. 31:40–51.
- Villareal DT, Fontana L, Weiss EP, Racette SB, Steger-May K, et al. 2006. Bone mineral density response to caloric restriction-induced weight loss or exercise-induced weight loss: a randomized controlled trial. *Arch Intern Med*. 166:2502–2510.
- Weindruch R, Gottesman SR, Walford RL. 1982. Modification of age-related immune decline in mice dietarily restricted from or after midadulthood. *Proc Natl Acad Sci USA*. 79:898–902.
- Weiss EP, Racette SB, Villareal DT, Fontana L, Steger-May K, et al.; Washington University School of Medicine CALERIE Group. 2007. Lower extremity muscle size and strength and aerobic capacity decrease with caloric restriction but not with exercise-induced weight loss. *J Appl Physiol*. 102:634–640.
- Westfall PH, Young SS, Wright SP. 1993. On adjusting P-values for multiplicity. *Biometrics*. 49:941.

Wright KM, Deighan A, Francesco AD, Freund A, Jovic V, et al. 2020. Age and diet shape the genetic architecture of body weight in diversity outbred mice. bioRxiv. 2020 doi: 10.1101/2020.11.04.364398.

Yu BP, Masoro EJ, McMahan CA. 1985. Nutritional influences on aging of Fischer 344 rats: I. Physical, metabolic, and longevity characteristics. J Gerontol. 40:657–670.

Communicating editor: J. Wolf